Effects of Surface Roughness on Transient Viscoelastic Fluids Flow Driven by Peristaltic Pumping

Ashvani Kumar [a], Anjali Bhardwaj [a], Dharmendra Tripathi*[a]

[a]Department of Mathematics, National Institute of Technology Uttarakhand, Srinagar-246174, India.

Abstract

The study examines how sinusoidal surface roughness influences the behaviour of viscoelastic fluids transported through physiological vessels via peristaltic pumping, a critical mechanism in biological systems with industrial applications. Most of the biological surfaces are smooth however they are not completely smooth and some roughness is always present. To understand and examine the roughness effects and viscoelastic behaviour of fluids, a mathematical model is developed by incorporating the low Reynolds number and long-wavelength approximations. In this study, viscoelastic fluid behaviour is analysed by considering the Jeffrey fluid model. This study examines how the relaxation-to-retardation time ratio and surface roughness height influence the fluid flow properties, such as axial velocity, pressure gradient, pressure distribution, volumetric flow rate, and skin friction. Findings indicate that greater surface roughness height reduces the fluid flow, evidenced by lower axial velocity and volumetric flow rate, alongside a higher-pressure gradient. Conversely, an increase in surface roughness height elevates skin friction, highlighting the additional resistance encountered by the fluids. These findings are critical for optimizing the fluid transport systems that involve viscoelastic fluids, especially in applications where precise control of fluid dynamics is required. The insights gained from this study are particularly valuable for improving the analysis of fluid behaviour in medical diagnostics and other related fields.

Keywords: Surface roughness; Viscoelastic fluids; Peristalsis; Skin friction; Pressure distribution; streamlines.

1 Introduction

Viscoelastic fluids possess both viscous and elastic characteristics, allowing them to flow like liquids while also deforming and recovering like solids. Their behaviour is time-dependent, meaning their reaction to stress or strain changes over time. This combination of properties is vital in various industries, particularly in polymer processing, where a deep understanding of their behaviour is key to improving manufacturing processes. Metzner and Park [1] revealed a notable reduction in turbulent viscoelastic fluid flow characteristics and a decrease in drag coefficients. Joseph and Liao [2] explored the drag in viscoelastic fluids and examined potential flows for specific fluid models. Zhou and Papautsky [3] investigated how viscoelastic fluid dynamics, including competing forces and fluid rheology, influence particle and cell migration in microchannels, aiming to enhance microfluidic applications in diagnostics and research. The Jeffery fluid model describes the key understanding of viscoelastic fluid flow behaviors, particularly in microfluidic applications where understanding these interactions is vital. Akbar et al. [4] studied blood flow in a

* ✉ dtripathi@nituk.ac.in

tapered artery with stenosis using a Jeffrey fluid model, examining how non-Newtonian effects influence velocity, temperature, wall shear stress, and impedance. Hayat et al. [5] explored heat transfer for boundary layer viscoelastic fluid flow containing nanoparticles around a stretchable cylinder. Sharma et al. [6] investigated a two-layer viscoelastic fluid model in stenosed arteries, finding that wall-shear stress and flow resistance greater with stenosis height and minimal with relaxation time, while velocity drops with stenosis.

Peristalsis refers to the rhythmic contraction of muscles, which influences fluid transport similar to how Jeffrey fluids, with their non-Newtonian behaviour, affect flow in complex systems like stenosed arteries. Ishikawa et al. [7] explored microbial flora transport in the small intestine with peristalsis, highlighting the complex interactions within the digestive system. Misra and Pandey [8] provided a comprehensive overview of peristaltic transport mechanisms for physiological fluids, offering insights into the mathematical modelling and simulation of these processes. Rao and Mishra [9] investigated the power-law fluids driven by peristaltic transport in porous media. Hayat et al. [10] explored peristaltic transport in a Jeffrey fluid, analysing the flow dynamics and the effects of fluid properties. Nadeem and Akbar [11] explored the viscoelastic fluid (Jeffery fluid) flow through peristaltic transport phenomena with varying viscosity in an asymmetric channel, highlighting how viscosity variations impact flow characteristics. Pandey and Tripathi [12] developed a model for Jeffrey-fluid transportation by peristalsis, focusing on time-dependent behaviors. Akbar et al. [13] examined the flow of chyme in the small intestine through peristalsis influenced by magnetic field. Bhatti and Abbas [14] studied the simultaneous effects of slip and magnetic fields on peristaltic blood flow in a porous medium with a Jeffrey fluid model. Guo et al. [15] extended this work with the magnetic field impact on peristaltic flow using a fractional Jeffrey model within the porous media.

Surface roughness refers to the imperfections and variations from an ideally smooth surface on a material. Taylor et al. [16] explored how surface roughness affects fluid flow, providing a comprehensive review of past, present, and future perspectives on this subject. Their work underscores the importance of surface characteristics in modifying fluid behaviour. Riaz et al. [17] presented an exact solution for the peristaltic flow of a Jeffrey fluid model within a three-dimensional rectangular duct, considering slip conditions at the walls. Surface roughness affects peristalsis by disrupting smooth fluid flow and introducing additional friction and turbulence. Shukla et al. [18] explored surface roughness effect on peristaltic pumping models, providing insights into how roughness alters the flow dynamics in such systems. Kotnurkar and Kallolikar [19] analysed the combined effects of electro-osmosis and induced magnetic fields on the peristaltic flow of Eyring Powell nanofluids in asymmetric channels, further emphasizing the complexities introduced by surface irregularities. Asghar et al. [20] offered an exact solution for cell movement over a Jeffrey slime layer, considering the impact of surface roughness, contributing to the understanding of cellular dynamics in biological environments. Additional studies by Shukla et al. [21] and Tanveer et al. [22] extended this research by examining heat transfer and Williamson nanofluid flow on rough surfaces, respectively, underscoring the critical role of surface roughness in fluid mechanics. Vaidya et al. [23] investigated the

peristaltic flow of Jeffrey fluid through an inclined tube, incorporating slip, variable viscosity, and thermal conductivity. Their MATLAB simulations revealed enhanced velocity, temperature, and bolus magnitude distributions. Choudhari et al. [24] examined the impact of wall slip on third-grade liquid flow in an inclined peristaltic channel. Their analysis considered variable viscosity, thermal conductivity, and wall properties, demonstrating that increased slip and viscosity led to enhanced velocity and bolus size. This study highlighted the complex rheology of blood in micro arteries.

The current research investigates the influence of surface roughness on the behaviour of viscoelastic fluids modulated by peristalsis. This study introduces the novel aspect of analysing viscoelastic fluids behaviour for rough surfaces. The influence of key parameters, such as viscoelastic fluid flow properties and surface roughness, is analysed on flow characteristics, including axial velocity, pressure gradient, pressure distribution, skin friction, volumetric flow rate, and stream function. MATLAB software is utilized for graphical representation of these flow characteristics. This study will be helpful to provide valuable insights in medical devices, industrial processes, and bioengineering, where understanding fluid dynamics in rough, non-Newtonian environments is crucial.

2   Mathematical formulation

2.1 Problem Definition

This analysis examines the flow of viscoelastic fluids within a peristaltically modulated channel featuring sinusoidal surface roughness. A sinusoidal wave travels along the channel walls with a wave velocity c. The wall geometry, illustrated in Fig. 1, is described as:

$$H(x^*, t^*) = a + b \sin\left(\frac{2\pi(x^* - ct^*)}{\lambda}\right) - b_1^* \cos\left(\frac{\pi x^*}{\beta_1^*}\right). \tag{1}$$

In this context, a represents the channel's half-width, while b and λ denote the wave's amplitude and wavelength respectively, β_1^* represents the pitch, b_1 denotes surface roughness height, L denotes the length of the channel, x^* represents axial variable, and t^* represents time.
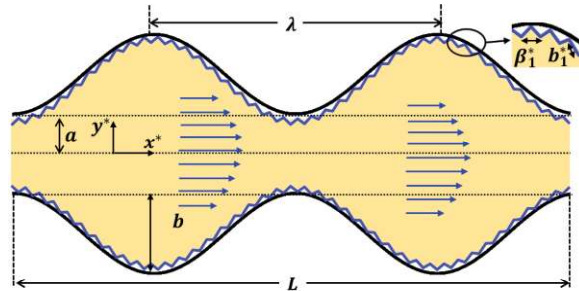

Figure 1: Graphical representation of peristaltic transport with surface roughness.

2.2 Jeffery Fluid Model

The fundamental equations for the extra stress τ^* for Jeffery fluid are expressed as follows:

$$\tau^* = \frac{\mu}{(1+\lambda_1)}\left(1 + \lambda_2 \frac{\partial}{\partial t^*}\right)\dot{\gamma} \tag{2}$$

Here, $\mu, \dot{\gamma}, \lambda_1$ and λ_2 represent the viscosity, strain rate, Jeffery fluid parameter (which is the ratio of relaxation time to retardation time), and the retardation time, respectively. The dots indicate derivatives with respect to time.

2.3 Governing Equations

The flow of Jeffery fluid within a peristaltically modulated microchannel, which has a rough surface, is governed by the following two-dimensional equations:

$$\frac{\partial u^*}{\partial x^*} + \frac{\partial v^*}{\partial y^*} = 0, \tag{3}$$

$$\rho\left(\frac{\partial}{\partial t^*} + u^*\frac{\partial}{\partial x^*} + v^*\frac{\partial}{\partial y^*}\right)u^* = -\frac{\partial p^*}{\partial x^*} + \frac{\partial \tau_{x^*x^*}^*}{\partial x^*} + \frac{\partial \tau_{x^*y^*}^*}{\partial y^*}, \tag{4}$$

$$\rho\left(\frac{\partial}{\partial t^*} + u^*\frac{\partial}{\partial x^*} + v^*\frac{\partial}{\partial y^*}\right)v^* = -\frac{\partial p^*}{\partial y^*} + \frac{\partial \tau_{y^*y^*}^*}{\partial y^*} + \frac{\partial \tau_{y^*x^*}^*}{\partial x^*}. \tag{5}$$

Here, ρ, u^*, v^*, p^*, x^*, y^* represent the fluid density, axial velocity, transverse velocity, pressure, axial coordinate and transverse coordinate respectively. To simplify

the governing equations mentioned above, certain non-dimensional parameters are introduced such as:

$$x = \frac{x^*}{\lambda}, y = \frac{y^*}{a}, t = \frac{ct^*}{\lambda}, u = \frac{u^*}{c}, v = \frac{v^*}{c\delta}, H = \frac{H^*}{a}, p = \frac{p^*a^2}{\mu c\lambda}, Re = \frac{\rho ca\delta}{\mu}, \tag{6}$$

$$\delta = \frac{a}{\lambda} \; \phi = \frac{b}{a}, \phi_1 = \frac{b_1^*}{a}, \beta_1 = \frac{\beta_1^*}{\lambda}, \tau = \frac{a\tau^*}{\mu c}.$$

By applying these non-dimensional parameters, the lubrication approximation is employed for the low Reynolds number and a long wavelength, specifically when $Re\delta \ll 1$. Once the lubrication approach is applied λ_2 is diminished and the governing equations can be expressed as follows:

$$\frac{\partial u}{\partial x} + \frac{\partial v}{\partial y} = 0, \tag{7}$$

$$\frac{\partial p}{\partial x} = \frac{1}{1+\lambda_1}\frac{\partial^2 u}{\partial y^2}, \tag{8}$$

$$\frac{\partial p}{\partial y} = 0. \tag{9}$$

The no-slip boundary conditions are used to solve these governing equations, which are given as follows:

$$u|_{y=H} = 0, \frac{\partial u}{\partial y}\Big|_{y=0} = 0, v|_{y=0} = 0, v|_{y=H} = \frac{\partial H}{\partial t}. \tag{10}$$

The axial and transverse velocities are derived by simplifying Eqs. (7-9) using the boundary conditions outlined in Eq. (10) as follows:

$$u = \frac{1+\lambda_1}{2}\frac{\partial p}{\partial x}(y^2 - H^2), \tag{11}$$

$$v = \frac{y(1+\lambda_1)}{6}\left\{6H\frac{\partial H}{\partial x}\frac{\partial p}{\partial x} - \frac{\partial^2 p}{\partial x^2}(y^2 - 3H^2)\right\}. \tag{12}$$

By using boundary condition $v|_{y=H} = \frac{\partial H}{\partial t}$, the expression for wall deformation can be expressed as follows:

$$\frac{\partial H}{\partial t} = \frac{1+\lambda_1}{3}\left\{3H^2\frac{\partial H}{\partial x}\frac{\partial p}{\partial x} + H^3\frac{\partial^2 p}{\partial x^2}\right\}. \tag{13}$$

On integrating with respect to x, pressure gradient can be obtained as:

$$\frac{\partial p}{\partial x} = \left(\frac{3}{1+\lambda_1}\right)\frac{1}{H^3}\left\{G_0(t) + \int_0^x \frac{\partial H(s,t)}{\partial t} ds\right\}, \tag{14}$$

where, arbitrary constant $G_0(t)$ can be determined as:

$$G_0(t) = \frac{\Delta p_L - \frac{3}{1+\lambda_1}\int_0^L \left(H^{-3}\int_0^x \frac{\partial H(s,t)}{\partial t}ds\right)dx}{\frac{3}{1+\lambda_1}\int_0^L H^{-3}dx}. \tag{15}$$

The wall shear stress, which is the tangential force per unit area exerted by a fluid on the wall, can be determined as follows:

$$\tau_w = \frac{\partial u}{\partial y}\big|_{y=H} = H(1+\lambda_1)\frac{\partial p}{\partial x}. \tag{16}$$

Furthermore, skin friction, refers to the drag force caused by the viscosity of a fluid, is determined as:

$$C_f = \frac{\partial H}{\partial x}\frac{\partial u}{\partial y}\big|_{y=H} = H(1+\lambda_1)\frac{\partial H}{\partial x}\frac{\partial p}{\partial x}. \tag{17}$$

Volumetric flow rate is determined as:

$$Q = \int_0^H u\, dy = -\frac{1+\lambda_1}{3}\frac{\partial p}{\partial x}H^3. \tag{18}$$

Stream function is calculated by using the definition of stream function as:
$u = \frac{\partial \psi}{\partial y}, v = -\frac{\partial \psi}{\partial x}$ and it yields:

$$\psi = \frac{y(1+\lambda_1)}{6}(y^2 - 3H^2)\frac{\partial p}{\partial x}. \tag{19}$$

3 Results and Discussion

Present study explores the effects of the ratio of relaxation time to the retardation time and surface roughness height on fluid characteristics. The effect of surface roughness on flow behaviour is important for understanding how fluid properties change when the surfaces aren't smooth. To represent the fluid characteristics, the wall geometry is expressed in a non-dimensional form as:

$$H(x,t) = 1 + \phi\sin(2\pi(x - t)) - \phi_1\cos\left(\frac{\pi x}{\beta_1}\right). \tag{20}$$

The analysis examines fluid characteristics such as axial velocity, pressure gradient, pressure distribution, skin friction, and stream function for different values of the ratio of relaxation time to the retardation time (λ_1) and roughness height (ϕ_1) as follows:
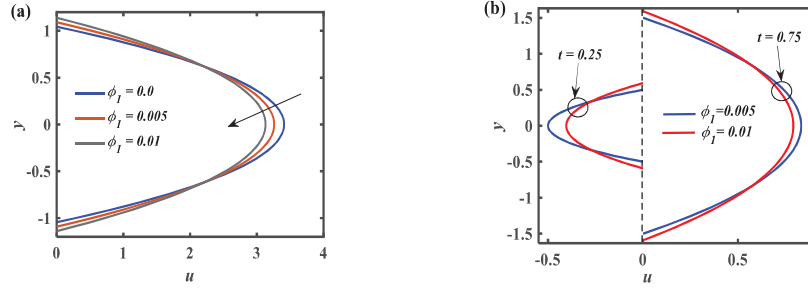
(a)

(b)

Figure 2: Variation in axial velocity for the various values of surface roughness height (ϕ_1) at different time phases (a) $t = 0.5$, (b) $t = 0.25, 0.75$.

Figs. 2(a&b) explore the changes in axial velocity across different roughness height values. Fig. 2(a) illustrates the behaviour of axial velocity at time $t = 0.5$ for various values of roughness heights. The findings show that an increase in roughness height leads to a reduction in axial velocity. Increasing surface roughness enhances flow resistance, thereby decreasing the axial velocity. Fig. 2(b) illustrates the changes in axial velocity at different times, specifically $t = 0.25$ and $t = 0.75$, for various roughness height values. The study demonstrates that an increase in roughness height leads to a reduction in velocity. Additionally, it is observed that at $t = 0.25$, the velocity graph shifts to the negative side, indicating that the fluid is moving in the backward direction at that time.
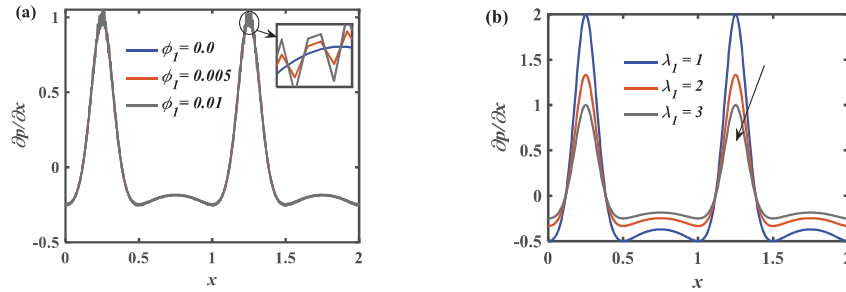
(a)

(b)

Figure 3: Variation in axial pressure gradient for the various values of (a) roughness height (ϕ_1), (b) ratio of relaxation time and retardation time (λ_1).

Figs. 3(a) and 3(b) illustrate the changes in the axial pressure gradient with varying values of roughness height and the ratio of relaxation to retardation time. Fig. 3(a) demonstrates that as the roughness height increases, the zig-zag pattern becomes more pronounced. Meanwhile, Fig. 3(b) shows that as the ratio of relaxation time to retardation time increases, the axial pressure gradient decreases. This implies that when the fluid has a higher relax stresses compared to its resistance to deformation (retardation), the flow encounters less resistance, leading to a reduction in the axial pressure gradient. Figs. 4(a&b) examine how pressure distribution changes with different values of roughness height and ratio of relaxation to retardation time. In Fig. 4(a), an increase in roughness height results in a higher-pressure distribution, indicating that greater surface roughness results in higher resistive forces within the microchannel. This increased resistance disrupts the flow more significantly. Conversely, Fig. 4(b) shows that an increase in the ratio of relaxation to retardation

time results in a decrease in the pressure distribution. This implies that fluids with a higher relaxation-to-retardation ratio experience less resistance and generate lower pressure distribution. Increased roughness height enhances resistive forces, critical for controlling flow rates in filtration or drug delivery. A higher relaxation-to-retardation ratio reduces axial pressure gradients and pressure distribution, beneficial for designing fluids that minimize energy losses in flow. These findings provide valuable guidance for optimizing channel designs and fluid properties to achieve efficient transport in various engineering and biomedical applications, including:- Microfluidics, Lab-on-a-chip systems, Point-of-care diagnostics, Biomedical devices, Filtration systems, Drug delivery systems. By leveraging these insights, researchers and engineers can develop innovative solutions that enhance fluid transport efficiency, reduce energy losses, and improve overall system performance.
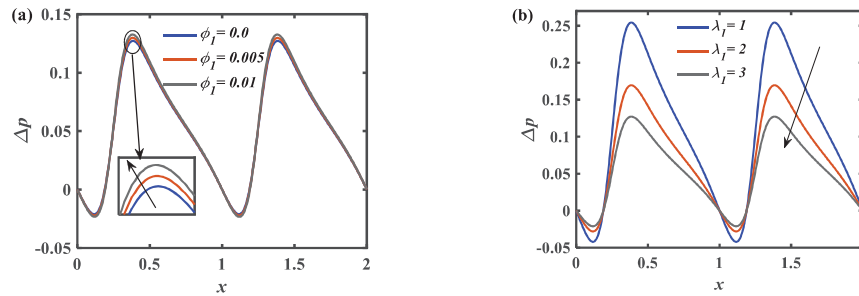

Figure 4: Variation in pressure distribution for the various values of (a) roughness height (ϕ_1), (b) ratio of relaxation time and retardation time (λ_1).
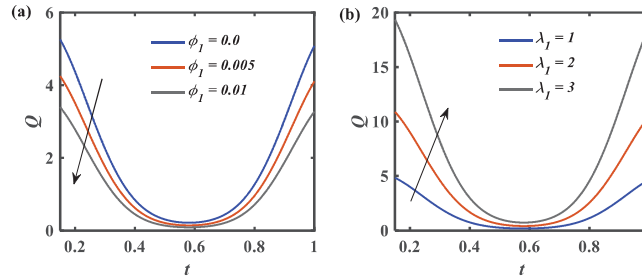

Figure 5: Variation in volumetric flow rate for the various values of (a) roughness height (ϕ_1), (b) ratio of relaxation time and retardation time (λ_1) at fixed position $x = 0.33$.

Figs. 5(a&b) examine how the volumetric flow rate changes over time at a fixed position $x = 0.33$ for varying values of roughness height and the ratio of relaxation to retardation time. Fig. 5(a) shows that an increase in roughness height leads to a decrease in volumetric flow rate. This occurs because higher roughness height increases resistance to fluid flow, thereby reducing the overall flow rate. On the other hand, Fig. 5(b) indicates that as the ratio of relaxation to retardation time increases, the volumetric flow rate also increases. Physically, this suggests that a higher ratio enhanced the fluid's ability to flowing at particular position within the microchannel. Higher relaxation-to-retardation ratio enhances flow, suggesting improved efficiency in systems involving viscoelastic fluids, such as lab-on-a-chip devices or biomedical fluid transport technologies, where precise control of fluid dynamics is critical.
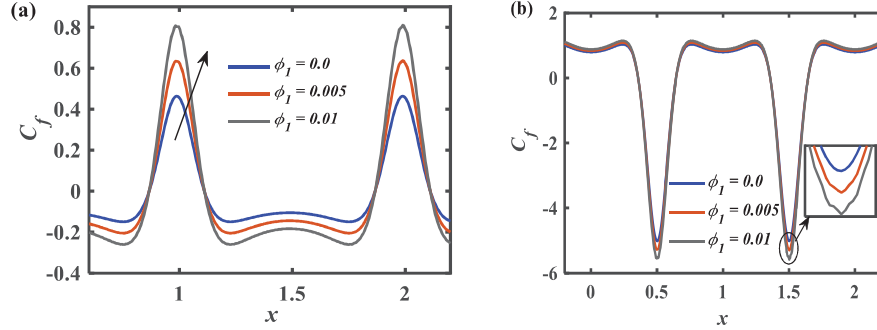
Figure 6: Variation in skin friction for the various values of roughness height (ϕ_1) at different time (a) $t = 0.25$, (b) $t = 0.75$.

Figs. 6(a&b) analysed the changes in skin friction for different roughness heights at two distinct time points, $t = 0.25$ and $t = 0.75$. The results show that an increase in roughness height leads to a rise in skin friction. Skin friction represents the resistance encountered by the fluid due to the interaction with the surface, and higher roughness height intensifies this resistance. This relationship highlights that as the surface becomes rougher, the frictional forces acting against the fluid flow increase, which can affect the overall fluid transport. Figs. 7(a-c present contour plots showing how axial velocity changes within the microchannel for roughness heights of $\phi_1 = 0.0, 0.01$ and $\phi_1 = 0.02$ at time $t = 0.5$. The figures reveal that as the roughness height increases, the magnitude of the axial velocity decreases. This indicates that greater surface roughness within the microchannel leads to a reduction in the flow speed. Roughness in the channel obstructs the flow, leading to a reduction in fluid movement as the roughness height increases, which in turn influences the overall fluid dynamics.
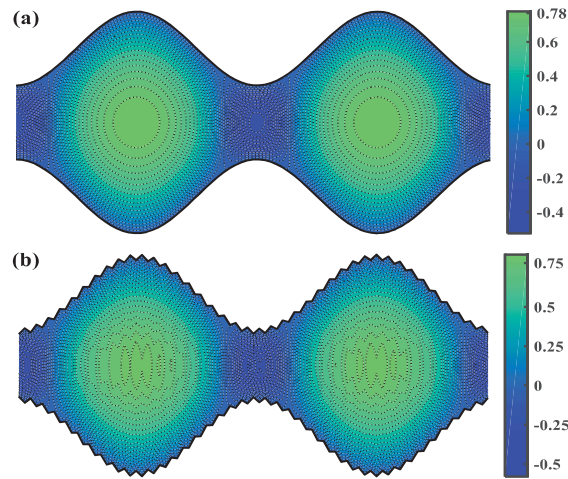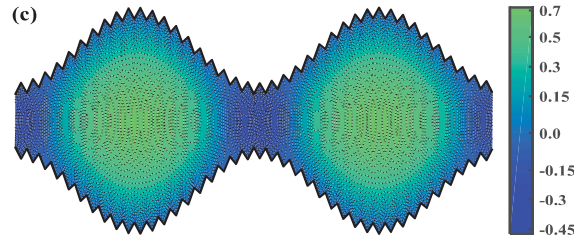
Figure 7: Contour plots of axial velocity for the various values of roughness height (a) $\phi_1 = 0.0$, (b) $\phi_1 = 0.01$, (c) $\phi_1 = 0.02$.

The findings of these studies have significant implications for various applications, including: Microfluidics: (Controlling flow resistance and directional velocity is crucial for optimizing microfluidic device performance, particularly in lab-on-a-chip systems and point-of-care diagnostics), Biomedical devices (Understanding peristaltic flows and fluid transport behaviour is essential for designing and optimizing biomedical devices, such as blood pumps, ventilators, and drug delivery systems), and Lubrication systems (The insights gained from these studies can inform the design of lubrication systems, where controlling flow resistance and directional velocity is vital for reducing friction and wear, and improving overall system efficiency). By optimizing flow resistance and directional velocity, these applications can achieve improved performance, efficiency, and reliability, ultimately leading to breakthroughs in fields such as healthcare, energy, and transportation.

4 Conclusions

Present study underscores the importance of considering surface roughness in microchannel flow analysis, as it plays a crucial role in shaping the overall fluid dynamics, including velocity, pressure distribution, and frictional forces. The impact of surface roughness on the flow of Jeffery fluid driven by peristalsis within a microchannel, leading to several key findings. It shows that as the surface roughness height increases, the axial velocity and volumetric flow rate decrease, while the axial pressure gradient and skin friction increase. These changes indicate that greater surface roughness introduces more resistance to the fluid flow. Furthermore, the study shows that as the ratio of relaxation time to retardation time increases, both the axial pressure gradient and pressure distribution decrease but volumetric flow rate increases. This suggests that fluids with higher relaxation capabilities experience less resistance during flow. These findings highlight the significant influence of surface roughness and the ratio of relaxation time to the retardation time on the flow characteristics within a microchannel. These insights are vital for optimizing the fluid flow in applications where surface roughness and fluid behaviour are applicable particularly in the biological flow phenomena. The present model is a basic model for the viscoelastic fluids flow driven by peristalsis with surface roughness however further extension of this model with other viscoelastic and viscoplastic fluids models, can be made for better analysis on various rheological characteristics of fluids and geometrical properties of physiological vessels and other flow regimes.

References

[1]   Metzner, A. B. and Park M. G., "Turbulent flow characteristics of viscoelastic fluids", *Journal of Fluid Mechanics,* vol. 20(2), pp. 291—303, 1964.

[2]   Joseph D. D. and Liao T. Y., "Potential flows of viscous and viscoelastic fluids" *Journal of Fluid Mechanics*, vol. 265, pp. 1—23, 1994.

[3]   Zhou J. and Papautsky I., "Viscoelastic microfluidics: Progress and challenges", *Microsystems & Nanoengineering,* vol. 6(1), p.113, 2020.

[4]   Akbar N. S. and Nadeem S., "Simulation of variable viscosity and Jeffrey fluid model for blood flow through a tapered artery with a stenosis", *Communications in Theoretical Physics,* vol. 57(1), p.133, 2012.

[5]   Hayat T., Asad S., and Alsaedi A., "Analysis for flow of Jeffrey fluid with nanoparticles", *Chinese Physics B*, vol. 24(4), p. 044702, 2015.

[6]   Sharma B. D., Yadav P. K., and Filippov A., "A Jeffrey-fluid model of blood flow in tubes with stenosis", *Colloid Journal*, vol. 79, pp. 849-856, 2017.

[7]   Ishikawa T., Sato T., Mohit G., Imai Y., and Yamaguchi T., "Transport phenomena of microbial flora in the small intestine with peristalsis", *Journal of Theoretical Biology*, vol. 279(1), pp. 63—73, 2011.

[8]   Misra J. C. and Pandey S. K., "Peristaltic transport of physiological fluids", In *Biomathematics: Modelling and Simulation*, pp. 167-193. 2006.

[9]   Rao A. R., and Mishra M., "Peristaltic transport of a power-law fluid in a porous tube", *Journal of Non-Newtonian Fluid Mechanics*, vol. 121(2-3), pp. 163—174, 2004.

[10]   Hayat T., Ali N., and Asghar S., "An analysis of peristaltic transport for flow of a Jeffrey fluid", *Acta Mechanica,* vol. 193, pp. 101—112, 2007.

[11]   Nadeem S. and Akbar N. S., "Peristaltic flow of a Jeffrey fluid with variable viscosity in an asymmetric channel", *Zeitschrift für Naturforschung A,* vol. 64 (11), pp. 713—722, 2009.

[12]   Pandey S. K. and Tripathi D., "Unsteady model of transportation of Jeffrey-fluid by peristalsis", *International Journal of Biomathematics,* vol. 3(4), pp. 473—491, 2010.

[13]   Akbar N. S., Nadeem S., and Lee C., "Characteristics of Jeffrey fluid model for peristaltic flow of chyme in small intestine with magnetic field", *Results in Physics*, vol. 3, pp. 152—160, 2013.

[14]   Bhatti M. M. and Abbas M. A., "Simultaneous effects of slip and MHD on peristaltic blood flow of Jeffrey fluid model through a porous medium", *Alexandria Engineering Journal*, vol. 55(2), pp. 1017—1023, 2016.

[15]   Guo X., Zhou J., Xie H., and Jiang Z., "MHD peristaltic flow of fractional Jeffrey model through porous medium", *Mathematical Problems in Engineering*, vol. 2018(1), p. 6014082, 2018.

[16]   Taylor J. B., Carrano A. L., and Kandlikar S. G., "Characterization of the effect of surface roughness and texture on fluid flow—past, present, and future", *International Journal of Thermal Sciences,* vol. 45(10), pp. 962—968, 2006.

[17]   Riaz A., Nadeem S., Ellahi R., and Zeeshan A., "Exact solution for peristaltic flow of Jeffrey fluid model in a three-dimensional rectangular duct having slip at the walls", *Applied Bionics and Biomechanics*, vol. 11(1-2), pp. 81—90, 2014.

[18] Shukla, R., Medhavi A., Bhatt S. S., Kumar R., and Tripathi D., "Surface roughness analysis on the peristaltic pumping flow model", *Pramana,* vol. 96(2), p. 89, 2022.

[19] Kotnurkar A. and Kallolikar N., "Effect of surface roughness and induced magnetic field on electro-osmosis peristaltic flow of Eyring Powell nanofluid in a tapered asymmetric channel", *Journal of Advanced Research in Numerical Heat Transfer,* vol. 10(1), pp. 20—37, 2022.

[20] Asghar Z., Elmoasry A., Shatanawi W., and Gondal M. A., "An exact solution for directional cell movement over Jeffrey slime layer with surface roughness effects", *Physics of Fluids,* vol. 35(4), 2023.

[21] Shukla R., Kumar A., Medhavi A., and Tripathi D., "Heat transfer and surface roughness analysis via peristaltic pumping of viscous fluids through diverging tube", *Numerical Heat Transfer, Part A: Applications,* pp. 1—21, 2024.

[22] Tanveer A., Rasheed I., and Jarral S., "Peristaltic flow of Williamson nanofluid on a rough surface", *Advances in Mechanical Engineering*, vol. 16(1), p. 16878132231222793, 2024.

[23] Vaidya H., Makinde O. D., Choudhari R., Prasad K. V., Khan S. U., and Vajravelu K., "Peristaltic flow of non-Newtonian fluid through an inclined complaint nonlinear tube: application to chyme transport in the gastrointestinal tract", *The European Physical Journal Plus,* vol. 135(11), pp. 1—15, 2020.

[24] Choudhari R., Makinde O. D., Mebarek-Oudina F., Vaidya H., Prasad H. V., and Devaki P., "Analysis of third-grade liquid under the influence of wall slip and variable fluid properties in an inclined peristaltic channel", *Heat Transfer,* vol. 51(7), pp. 6528—6547, 2022.